

# Description and Analysis of New Motion Conversion Mechanism for Heavy-Loaded Reciprocating Pumps

J. H. Sol, *Member, IAENG*

**Abstract**—In this paper a new mechanism for the conversion of reciprocating motion into rotary motion and vice versa is described and analyzed. In this analysis the new type of mechanism is applied in a reciprocating pump application. It is found that the mechanism significantly reduces unfavorable radial forces which subsequently result in a more efficient motion conversion. Also, evaluation of the mechanism's geometry leads to the conclusion that this mechanism is better able to withstand heavy shock loads compared to existing mechanisms for the conversion of reciprocating motion into rotational motion. In addition, various configurations of the mechanism are described.

**Index Terms**—Motion conversion, reciprocating pumps, crankshaft, energy efficiency.

## I. INTRODUCTION

THE conversion of reciprocating motion into rotary motion in heavy-loaded reciprocating pumps is currently performed by a crankshaft or an eccentric mechanism. Although these mechanisms performed well during recent decades, increasing mechanical problems arise due to the increasing pressure and displacement requirements partly accelerated by the shale gas revolution[1].

In a response to these increasing demands for pumps that are able to withstand extreme pressures, pump manufacturers straightforwardly increase their crankshafts in size which results in excessively large and heavy mechanisms which remain sensitive to mechanical (fatigue) failures due to two fundamental weaknesses.

The first key weakness is the occurrence of critical stress concentrations anywhere a change in diameter exists. These stress concentrations are prone to fatigue failures, especially under high shock loadings such as takes place in reciprocating pumps and combustion engines[2]. The second weakness in the current mechanisms is the limited allowable wrist pin bearing load. This is caused by the limited space available for increasing bearing size and because this bearing is difficult to lubricate.

These two key weaknesses jointly restrict the maximum allowable load on the crankshaft mechanism. A modular eccentric mechanism suffers only from the limited wrist pin bearing load. A new motion conversion mechanism which is commercially known as the "Efficient Motion Converter" (also "EMC") doesn't have these weaknesses and should be able to withstand heavy shock loads. In this paper the

mechanism is presented and initial analyses are performed.

## II. DESCRIPTION OF MECHANISM

### A. Core components & motion

Although the new mechanism also consists out of a (modular) eccentric, the rest of the mechanism is completely different. An exploded view drawing of the mechanism is given in Fig. 1.

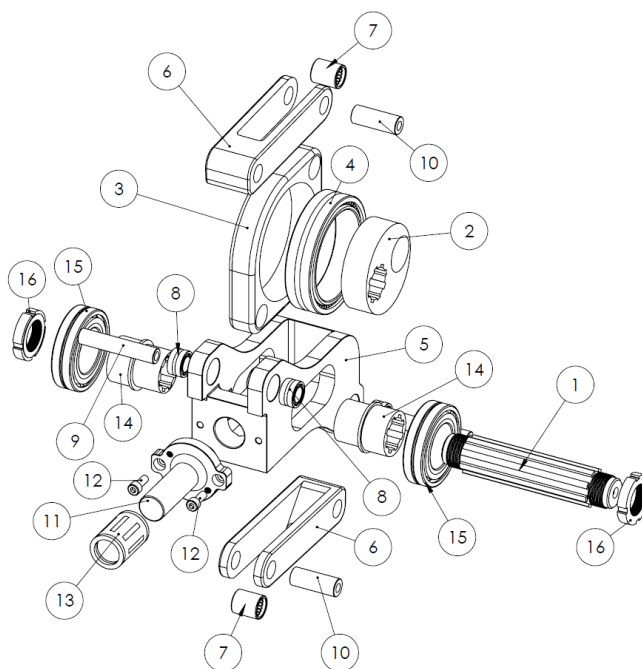


Fig. 1. Exploded view of the mechanism. Although the mechanism also consists out of a commonly used (modular) eccentric, various new components are introduced.

The core of the mechanism consists out of a modular eccentric which is mounted on a splined shaft (#1). The eccentric movement of the eccentric sheave (#2) is not transferred through a connection rod as usually, instead, this movement is transferred via a bearing (4#) to a bearing housing (#3) to two rods (#6). The other outer side of the hinging rods are connected to a reciprocating member (#5) which moves in a pure reciprocating way. On one end of the reciprocating member, or at both ends, a crosshead (#11) or other components can be connected which require to move in a reciprocating way. An illustration of the movement from top dead center to bottom dead center is given in Fig. 2.

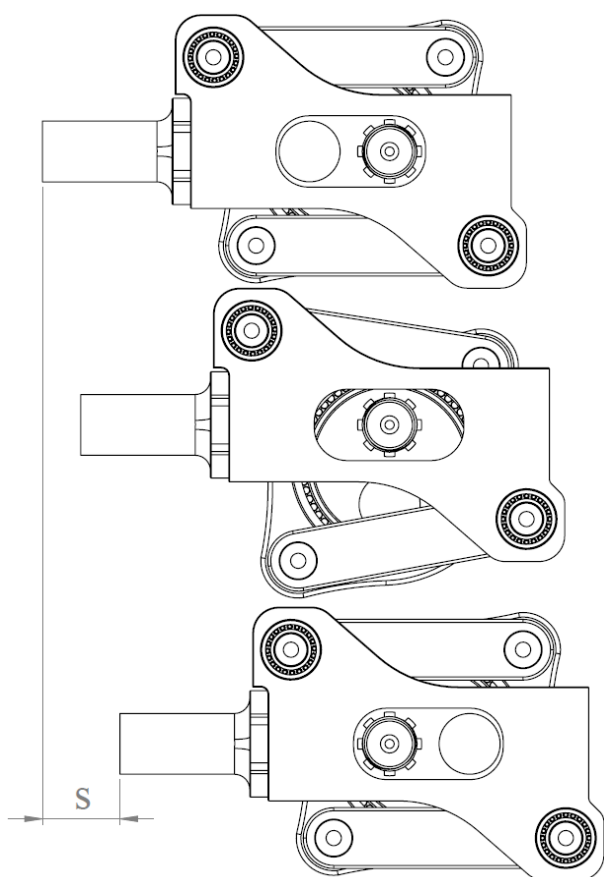


Fig. 2. Movement of the mechanism from top dead center to bottom dead center. The shaft rotates counter clockwise.

### III. ANALYSIS OF MECHANISM

#### A. Force analysis

In order to determine how the load is being transferred along the various components, a static state force analysis is performed. A crosshead load of 100 N is applied (being in the  $-Z$  direction) at a variety of shaft positions. In this analysis the shaft(#1) and the linear ball bearing (#13) were both fixed for rotation and translation. In Fig. 3 the various nodes are illustrated and in Fig. 4 the relevant dimensions are illustrated.

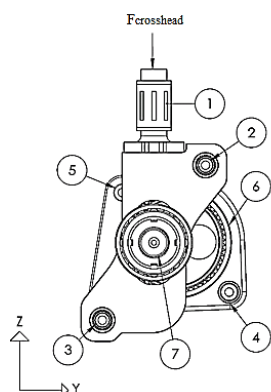


TABLE I		
Node / Contact	Description	Number of similar contacts
1	Reaction force crosshead (#11) / linear ball bearing (#13)	1
2	Reaction force wrist pin (#9) / needle bearing (#8) (upper case)	2
3	Reaction force wrist pin (#9) / needle bearing (#8) (lower case)	2
4	Reaction force wrist pin (#10) / needle bearing (#7) (lower case)	1
5	Reaction force wrist pin (#10) / needle bearing (#7) (upper case)	1
6	Reaction force needle bearing (#4) / bearing housing (#3)	1
7	Reaction force bearing bushing (#14) / main bearing (#15)	2

Fig. 3. Definition of contacts. Part numbers refer to figure 1.

From this analysis it is found that the reaction force in Y-direction on the crosshead (i.e. node 1) is far lower compared to the radial force induced by a crankshaft or eccentric mechanism. To illustrate, in a crank with a commonly used  $r/s$  ratio of 2.5 the maximum radial load on the crosshead is

more than 20% of the plunger load. In the new mechanism the maximum radial load is 10.5% of the plunger load. This is caused by the fact that the two connection rods (#6) which jointly transfer the plunger load to the bearing housing are pointing in opposite direction. Therefore the Y-forces of both rods cancel each other to a large extent out. All relative values can be found in Table IV in APPENDIX I.

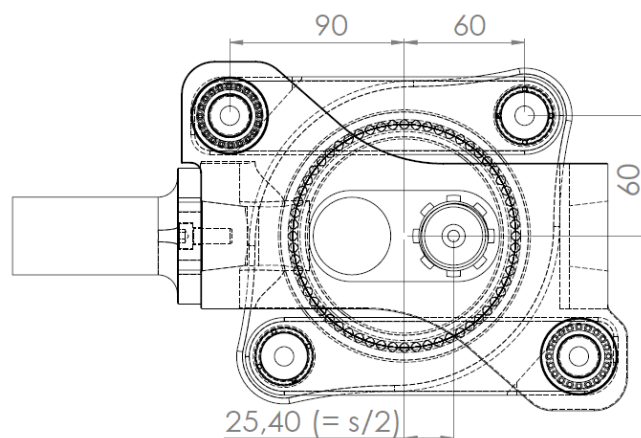


Fig. 4. Relevant dimensions for force and motion analysis.

#### B. Motion analysis

Motion analysis is performed on the new mechanism and compared with motion plots of a crank mechanism with a similar stroke (50.8 mm) and with a  $r/s$  ratio of 2.5. For the new mechanism the same geometry is used as in the force analysis.

Displacement, velocity and acceleration plots for both mechanisms are illustrated in Fig. 5., Fig. 6. and Fig 7. respectively. Measurements are done on top of the crosshead.

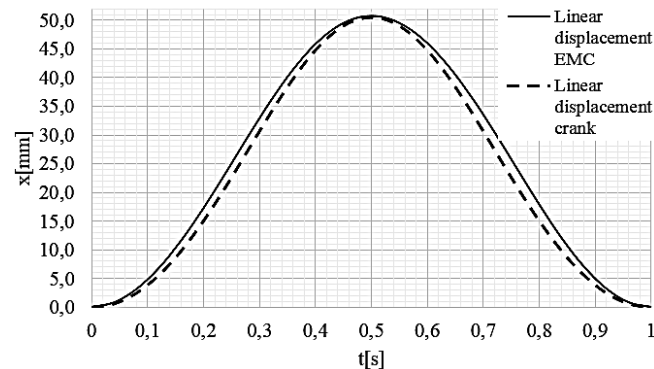


Fig. 5. Displacement plots of new mechanism, being the continuous curve, and conventional crank mechanism, being the dotted curve.

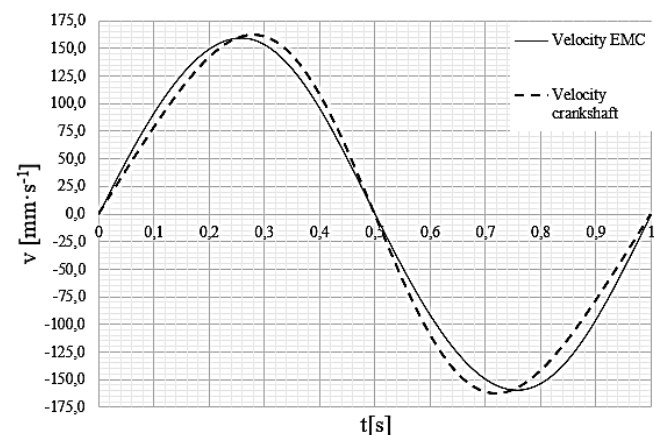


Fig. 6. Velocity plots of new mechanism, being the continuous curve, and conventional crank mechanism, being the dotted curve.

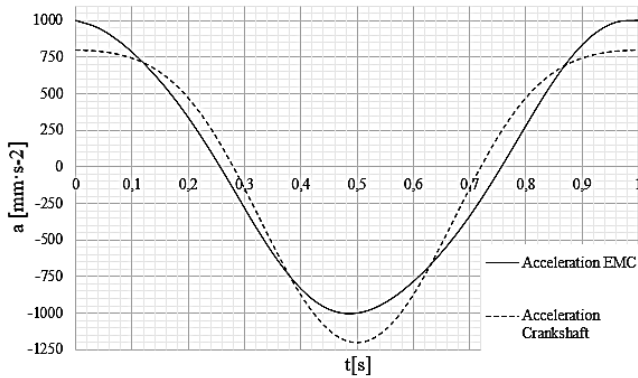


Fig. 7. Acceleration plots of new mechanism, being the continuous curve, and conventional crank mechanism, being the dotted curve.

In the motion plots the crosshead starts at bottom dead center and one cycle is completed at 1 sec..

It is found that there are significant differences in displacement, velocity and acceleration curves between the new mechanism and the crankshaft mechanism. From a reciprocating pump perspective especially the difference in acceleration is interesting as pump's maximum rotational frequency, and thereby are also pump's displacement, is partly restricted by plunger acceleration due to potential cavitation during the inlet phase. As the alternative mechanism has a significant lower acceleration (in this case 15,4% lower) during top dead center, risk of cavitation is significantly reduced at the same rotational frequency.

#### C. Analytical mechanical strength considerations

Although no FEA analyses are performed yet, initial analytical evaluations gain insight into the relative mechanical strength of the mechanism. Three observations regarding mechanical strength are of interest. The first observation is related to the wrist pin bearing. Normally the wrist pin bearing is the highest loaded bearing in a crankshaft / eccentric mechanism which is mainly caused by the limited available space for this bearing. The highest loaded bearings in the alternative mechanism are part #7 and part #8. These bearings are not restricted by available space and can therefore be chosen until a certain load level is achieved. Secondly, no critical change in diameters exist. In a crank various diameter changes exist in which stresses concentrate and which are prone to fatigue failures. The new mechanism doesn't have these stress inducing fillets and should therefore be better suited for high shock loadings. The third observation is specifically related to triplex pumps which consist out of a cast crank which is supported at both ends. The modularity of the new mechanism allows for adding main bearings between the eccentric webs which results in a great reduction in bending moment. Secondly, a straight shaft as applied in the EMC has a higher torsional rigidness than a crank with webs which subsequently results in lower torsional stresses.

#### D. Conversion efficiency analysis

The mechanical efficiency of the mechanism under investigation can be determined by the identification and calculation of friction losses caused by the bearings. In this analysis it is assumed that throughout the whole cycle a constant load is applied on the top of the plunger.

The total amount of work required to overcome the friction losses can be calculated with the following equation:

$$W_{\text{TotalFriction}} = W_{\text{Node 1}} + 2W_{\text{Node 2}} + 2W_{\text{Node 3}} + W_{\text{Node 4}} + W_{\text{Node 5}} + W_{\text{Node 6}} + 2W_{\text{Node 7}} \quad (1)$$

Node 1 consists of a linear ball bearing of which the friction work can be calculated as follows:

$$W_{\text{Node 1}} = F_{f1av} * \Delta x_1 \quad (2)$$

Herein represents  $\Delta x_1$  the relative translation between the crosshead and the linear ball bearing, which is equal to  $2s$ .  $F_{f1av}$  represents the average friction force between the crosshead and the linear ball bearing during one cycle. This average friction force can be calculated with the following formula:

$$F_{f1av} = F_{res1av} * \mu_{lbb} \quad (3)$$

$F_{res1av}$  can be calculated by integrating the trend line of the force plot of the resultant force of node 1.  $\mu_{lbb}$  represents the friction coefficient a linear ball bearing. Substituting (3) in (2) and replacing  $\Delta x_1$  by  $2s$  results in:

$$W_{\text{Node 1}} = F_{res1av} * \mu_{lbb} * 2s \quad (4)$$

Node 2 represents an oscillating needle bearing with a limited rotation angle. Friction work can be calculated by using the following equation:

$$W_{\text{Node 2}} = F_{f2av} * \Delta x_2 \quad (5)$$

Herein  $\Delta x_2$  represents the relative movement between the inner and the outer ring of the bearing while  $F_{f2av}$  represents the average friction force during one cycle.  $\Delta x_2$  can be calculated with the following equation:

$$\Delta x_2 = \pi * d_2 * \frac{2 * \theta_2}{360} \quad (6)$$

$\theta_2$  represents the angular displacement of the rod (part #6) relative to the reciprocating member (part #5) in the XZ plane (coordinate system of Fig. 3) during one cycle. As the rod starts in horizontal position, during one main shaft rotation the total angular displacement is equal to  $2 * \theta_2$ .  $d_2$  represents the mean diameter of the needle bearing.

Due to the relative constancy along the cycle  $F_{f2av}$  can be calculated by taking the average of the resultant force of node 2 during one cycle and multiply this figure with the friction coefficient of a needle bearing.

Substitution of (6) into (5) and replacement of  $F_{f2av}$  by  $F_{res2av}$  results in:

$$W_{\text{Node 2}} = F_{res2av} * \mu_{nb} * \pi * d_2 * \frac{2 * \theta_2}{360} \quad (7)$$

The friction losses of node 3, 4, 5 can be determined in a similar way as described for node 2.

The work required to overcome friction per cycle for node 6 can be calculated by:

$$W_{\text{Node 6}} = F_{f6av} * \pi * d_6 = F_{res6av} * \mu_{nb} * \pi * d_6 \quad (8)$$

$F_{res6av}$  represents the average resultant force on node 6,  $\mu_{nb}$  represents the friction coefficient of a needle bearing and  $d_6$  represents the average diameter of the needle bearing (part # 4).  $W_{\text{Node 7}}$  can be calculated in the same way by adjusting the

formula for the specific diameter, load and bearing specifications of node 7.

Combining equations (4), (7), (8) and rewriting these equations for similar nodes allows for replacing equation (1) by the following:

$$W_{TotalFriction} = (F_{res1av} * \mu_{lbb} * 2s) + 2(F_{res2av} * \mu_{nb} * \pi * d_2 * \frac{2 * \theta_2}{360}) + 2(F_{res3av} * \mu_{nb} * \pi * d_3 * \frac{2 * \theta_3}{360}) + (F_{res4av} * \mu_{nb} * \pi * d_4 * \frac{2 * \theta_4}{360}) + (F_{res5av} * \mu_{nb} * \pi * d_5 * \frac{2 * \theta_5}{360}) + (F_{res6av} * \mu_{nb} * \pi * d_6) + 2(F_{res7av} * \mu_{sb} * \pi * d_7) \quad (9)$$

This represents the total amount of work to overcome mechanical friction during one cycle. In order to calculate the mechanical efficiency of the mechanism this amount of friction work has to be compared with the total amount of work input during one cycle with a given load. This will be demonstrated in the following calculation example.

Calculation example

TABLE II  
VALUES VARIABLES

Variable	Value	Variable	Value
F <sub>plunger</sub>	20 kN	d <sub>5</sub>	22.5 mm
s	50.8 mm	d <sub>6</sub>	115 mm
θ <sub>2</sub> , θ <sub>3</sub> , θ <sub>4</sub> , θ <sub>5</sub>	19.5°	d <sub>7</sub>	76.5 mm
d <sub>2</sub>	23 mm	μ <sub>lbb</sub>	0.0025
d <sub>3</sub>	23 mm	μ <sub>nb</sub>	0.003
d <sub>4</sub>	22.5 mm	μ <sub>sb</sub>	0.0018

Before equation (9) can be applied the average loads on the various nodes have to be determined. For node 2, 3, 4, 5, 6, 7 this can be done straightforwardly by calculating the arithmetic mean of the various values of the various positions from Table IV. In order to determine the average load for node 1 the resultant force (for 0°-180° and for 180°-360° separately) have to be plotted where after a trend line can be added.

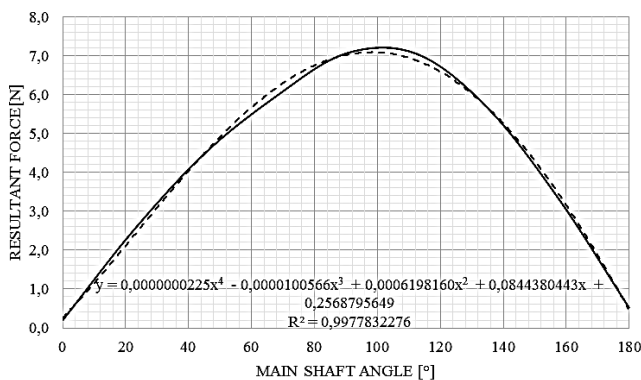


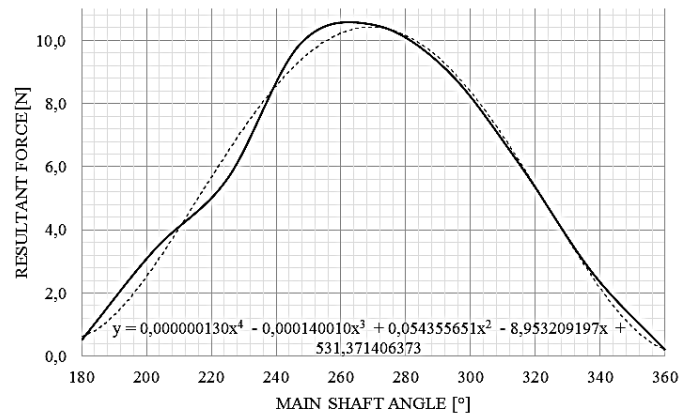
Fig. 8. Resultant force plot from 0° to 180° shaft angle at node 1, being the crosshead. 0° corresponds with top dead center plunger position. 4<sup>th</sup> order polynomial function is fitted as trend line.

Average resultant force from 0° to 180° is found by integrating the trend line function and dividing this definite integral value through 180.

$$F_{res1av0°-180°} = \frac{1}{180 - 0} \int_0^{180} (2 * 10^{-8}x^4 - 0.00001x^3 + 0.0006x^2 + 0.0844x + 0.2569)dx$$

$$F_{res1av0°-180°} = 4.61 \text{ [%]}$$

The same can be done for the second part of the cycle.



Graph 8 Resultant force plot from 180° to 360° shaft angle at node 1, being the crosshead. 180° corresponds with bottom dead center plunger position. 4<sup>th</sup> order polynomial function is fitted as trend line.

$$F_{res1av180°-360°} = \frac{1}{360 - 180} \int_{180}^{360} (1 * 10^{-7}x^4 - 0.0001x^3 + 0.0544 - 8.9532x + 531.37)dx$$

$$F_{res1av180°-360°} = 7.38 \text{ [%]}$$

The average resultant force at node 1 during one cycle can be calculated with:

$$F_{res1av} = \frac{F_{res1av0°-180°} + F_{res1av180°-360°}}{2} = \frac{4.61 + 7.38}{2} = 11.99 \text{ [%]}$$

As mentioned above, the average load on node 2, 3, 4, 5, 6, 7 can be calculated by taking the arithmetic average of the loads of the 9 crank positions. This results in the following values:

TABLE III  
AVERAGE LOADS DURING CYCLE

Node	Average load during cycle $F_{resav}$ [% of plunger load]	Absolute Average Load during cycle $F_{resav}$ [kN]
1	11.99%	2.24
2	25.58%	5.12
3	24.64%	4.93
4	51.10%	10.22
5	49.27%	9.85
6	99.78%	19.96
7	49.83%	9.97

Now equation (9) can be applied in order to calculate the mechanical efficiency:

$$W_{TotalFriction} = (2240 * 0.0025 * 2 * 0.0508) + 2 * (5120 * 0.003 * \pi * 0.023 * \frac{39}{360}) + 2 * (4930 * 0.003 * \pi * ...)$$

$$0.023 * \frac{39}{360}) + (10220 * 0.003 * \pi * 0.0225 * \frac{39}{360}) + \\ (9850 * 0.003 * \pi * 0.0225 * \frac{39}{360}) + (19960 * 0.003 * \pi * \\ 0.115) + 2 * (9970 * 0.0018 * \pi * 0.0765)$$

$$W_{TotalFriction} = 31.74 [Nm]$$

The total amount of work exerted on the plunger can be calculated with:

$$W_{Plunger} = F_{Plunger} * \Delta x = F_{Plunger} * 2 * s \\ = 20000 * 2 * 0.0508 = 2032 [Nm]$$

The mechanical efficiency of the mechanism can subsequently be determined by:

$$\eta_{mechanism} = \frac{W_{Plunger} - W_{TotalFriction}}{W_{Plunger}} = \frac{2032 - 31.74}{2032} \\ = 98.44 [\%]$$

In order to bring this number in perspective the efficiencies of a crank mechanism and eccentric mechanism are calculated as well. Using the same methodology and case data it is found that a normal crankshaft mechanism has a theoretical mechanical efficiency of 98.04% and an eccentric 97.38%. This means the EMC mechanism is 0.4% more efficient than a crank mechanism and 1.06% more efficient than an eccentric mechanism.

The efficiency gain can, for the greater part, be attributed to the lower frictional losses in the crosshead. This is caused by the lower normal force on the crosshead as well as the decreased friction coefficient (0.07(-) vs. 0.0025(-)) due to the introduction of the linear ball bearing instead of a normal crosshead configuration.

Please also note that these calculations do not take into account deformations due to the mechanical loads. This causes unfavorable misalignments which induce additional friction. It's likely that this is higher with a normal crankshaft than with the EMC as the EMC mechanism is a far more rigid mechanism.

#### IV. CONFIGURATIONS

##### A. Single configuration

The single configuration can be used for triplex pumps by placing three mechanisms in-line on the same main shaft. In this configuration four instead of two main bearings can be applied. This results in a significant reduction in bending moment and allows for a higher plunger load.

##### B. Boxer configuration

The boxer configuration allows for plunger installation at both ends of the mechanism. By doing this displacement or pressure capabilities can be doubled. Sideway forces can be absorbed at one side of the mechanism by installing a linear ball bearing while at the other side a pony rod can be installed directly. An illustration of this mechanism is given in Fig. 9.

##### C. Combination combustion cycle – pump cycle

Another possible configuration is to use the mechanism in a dual role between combustion engine and pump. This dual role entails that at one side of the mechanism work is being added by an internal combustion engine cycle while at the

other side of the mechanism work is being retracted by a reciprocating pump configuration. In this configuration the forces induced by the combustion are directly being transferred to the plunger that is being used for pump purposes and therefore a minimal residual force is being transferred to the oscillating and rotating members.

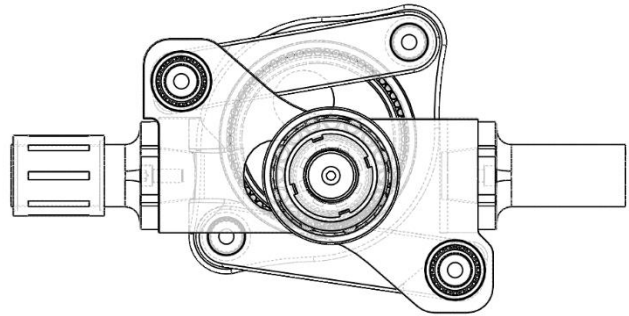


Fig. 9. New mechanism configured as boxer configuration.

This configuration brings along a variety of advantages. Firstly, the (residual) forces on the bearings are strongly reduced which leads to lower friction losses and a higher reliability. Secondly, no drive motor and transmission is required anymore which further increases efficiency, reliability and also simplicity. Thirdly, total system size and weight can be reduced significantly.

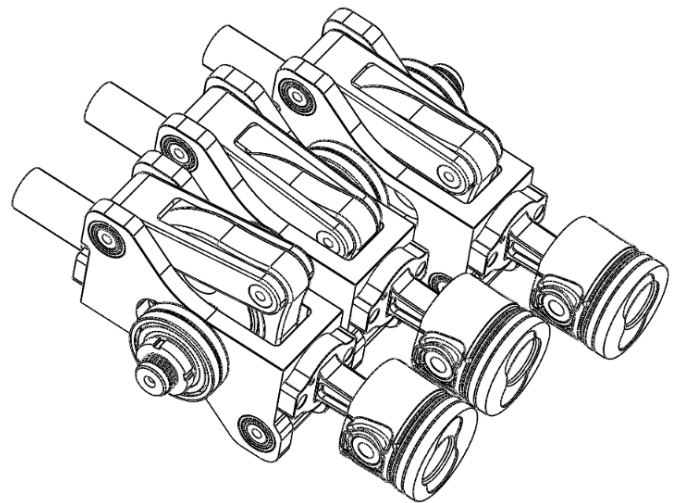


Fig. 10. New mechanism allows for a dual role between combustion cycle and pump cycle.

##### General considerations on combined configuration

For this first evaluation ideal conditions and processes are assumed. A first requirement for this configuration is that the amount of work that is retracted by the pump has to be equal to the amount of work that is added by the combustion cycle. This can be written as:

$$\sum W = W_{net\_combustion} - W_{pump} = 0 \quad (10)$$

In combustion engine terminology the average effective pressure over one cycle is known as I.M.E.P. (Indicated Mean Effective Pressure). A typical IMEP value for a boosted two-stroke gasoline engine is about 15 bar [3]. This means that in case an equal stroke and plunger diameter for both sides is used, plunger pressure is limited to 15 bar. However, pump plunger and combustion piston size don't have to be the same; the combustion piston can have a (far) greater surface than

the plunger diameter. For example, if the plunger diameter is decreased 1.5 times and the combustion piston is increased 1.5 times the plunger pressure can be increased up to 76 bar.

There are however limitations to the extent to which the diameters can be adjusted. Due to specific combustion engine characteristics the ratio between bore and stroke of the combustion piston is limited to about 2 [4]. It is however doubtful whether this limit also applies in case the new mechanism is applied as this limit is partly caused by mechanical limitations. As these mechanical limitations might not apply in case the new mechanism is applied further research should be done to investigate which bore-to-stroke ratios are possible.

The amount of work that is delivered during the expansion stroke,  $W_{expansion}$ , should be equal to the amount of work that is required for the pump, being  $W_{pump}$ , plus the amount of work that is required for compression of the air-fuel mixture, being  $W_{compression}$ . When the combustion piston travels from top dead center to bottom dead center the first work factor, being  $W_{pump}$ , is directly transferred via the reciprocating member to the plunger while the remaining amount of work, being  $W_{compression}$ , is temporarily stored in the flywheel. When the combustion piston travels back from the bottom dead center to the top dead center the work stored in the flywheel has to be transferred back in order to compress the air-fuel mixture. This means that during the whole cycle the mechanism is only loaded with the forces related to the air-fuel mixture compression and not with the forces related to the pump compression. This subsequently means a significant reduction in load on all parts which results in a higher efficiency and allows for a lighter construction.

The most favorable configuration would include a 2-stroke Otto cycle. A two-stroke cycle delivers one power stroke per shaft cycle while a four-stroke deliver one power-stroke per two shaft cycles. This means that with a four stroke cycle lower pump pressures can be achieved and also more energy has to be stored in the flywheel which undo the low forces advantage. Also, an Otto cycle is preferred to a Diesel cycle. The Otto-cycle has a far lower pressure at the end of the compression stroke compared to a Diesel cycle. The forces resulting from compression are the highest forces in the mechanism during the cycle and should therefore be minimized. Consequently, an Otto cycle is preferred to a Diesel cycle although both cycles are feasible.

### V. FUTURE RESEARCH

An initial analysis is performed on the mechanism in a reciprocating pump application. A further in-depth analysis on strength, vibration and lubrication is required for determining the feasibility and attractiveness of the mechanism. Also the combined combustion configuration deserves a further in-depth feasibility analysis. In this analysis mainly the timings of the various forces should be explored in more detail.

## APPENDIX I

TABLE IV(a)

Angular shaft position [°]	Node 1			Node 2			Node 3		
	Y-direction	Z-direction	Resultant	Y-direction	Z-direction	Resultant	Y-direction	Z-direction	Resultant
0	0,2%	0,0%	0,2%	0,2%	25,1%	25,1%	0,1%	24,8%	24,8%
45	4,5%	0,0%	4,5%	4,0%	24,2%	24,5%	1,8%	25,7%	25,8%
90	7,1%	0,0%	7,1%	5,8%	24,4%	25,1%	2,3%	25,4%	25,5%
135	5,7%	0,0%	5,7%	4,3%	24,6%	24,9%	1,5%	25,3%	25,4%
180	0,5%	0,0%	0,5%	0,4%	25,2%	25,2%	0,0%	24,7%	24,7%
225	5,6%	0,0%	5,6%	4,3%	24,6%	25,0%	1,5%	25,3%	25,3%
270	10,5%	0,0%	10,5%	7,0%	27,3%	28,1%	1,7%	22,6%	22,6%
315	6,1%	0,0%	6,1%	4,6%	26,1%	26,5%	1,5%	23,7%	23,8%
360	0,2%	0,0%	0,2%	0,2%	25,1%	25,1%	0,1%	24,8%	24,8%

Fig. 11. Forces at various main shaft positions for node 1, node 2, node 3.

TABLE IV(b)

Angular shaft position [°]	Node 4			Node 5			Node 6		
	Y-direction	Z-direction	Resultant	Y-direction	Z-direction	Resultant	Y-direction	Z-direction	Resultant
0	0,5%	50,1%	50,1%	0,3%	49,5%	49,5%	0,2%	99,6%	99,6%
45	8,1%	48,3%	49,0%	3,6%	51,3%	51,5%	4,5%	99,6%	99,7%
90	11,6%	48,8%	50,1%	4,6%	50,9%	51,1%	7,1%	99,6%	99,9%
135	8,6%	49,1%	49,8%	2,9%	50,5%	50,6%	5,7%	99,6%	99,8%
180	0,7%	50,3%	50,3%	0,2%	49,4%	49,4%	0,5%	99,6%	99,6%
225	8,6%	49,2%	49,9%	3,0%	50,4%	50,5%	5,6%	99,6%	99,8%
270	13,9%	54,5%	56,3%	3,4%	45,1%	45,2%	10,5%	99,6%	100,0%
315	9,2%	52,2%	53,0%	3,1%	47,5%	47,6%	6,1%	99,6%	99,8%
360	0,5%	50,1%	50,1%	0,3%	49,5%	49,5%	0,2%	99,6%	99,6%

Fig. 12. Forces at various main shaft position for node 4, node 5, node 6.

TABLE IV(c)

Angular shaft position [°]	Node 7		
	Y-direction	Z-direction	Resultant
0	0,1%	49,8%	49,8%
45	1,3%	49,9%	49,9%
90	0,5%	49,8%	49,8%
135	1,1%	49,8%	49,8%
180	0,0%	49,8%	49,8%
225	0,9%	49,8%	49,9%
270	0,2%	49,8%	49,8%
315	1,5%	49,8%	49,9%
360	0,1%	49,8%	49,8%

Fig. 13. Forces at various main shaft positions for node 7

## NOMENCLATURE

Symbol	Quantity	Unit
a	Acceleration	mm·s <sup>-2</sup>
d	Diameter	mm
F	Force	N
Fr	Friction force	N
Fres	Resultant force	N
r	Center distance between small-end center and big-end center	mm
s	Stroke	mm
v	Velocity	mm·s <sup>-1</sup>
W	Work	Nm
x	Displacement	mm
θ	Angular displacement	°
μ <sub>lbb</sub>	Friction coefficient linear ball bearing	-
μ <sub>sb</sub>	Friction coefficient spherical bearing	-
μ <sub>nb</sub>	Friction coefficient needle bearing	-

## REFERENCES

- [1] The Evolution of Hydraulic Fracturing and its Effect on Frac Pump Technology. Available at: <http://www.pump-zone.com/topics/upstream-pumping/evolution-hydraulic-fracturing-and-its-effect-frac-pump-technology> Retrieved 25 March 2014.
- [2] Espadafor, F. J., Villanueva, J. B., & García, M. T. (2009). Analysis of a diesel generator crankshaft failure. *Engineering Failure Analysis*, 16(7), 2333-2341.
- [3] J. B. Heywood, *Internal Combustion Engine Fundamentals*. McGraw-Hill, New York (1988).
- [4] Siewert, R., "Engine Combustion at Large Bore-to-Stroke Ratios," *SAE Technical Paper*, 780968, *SAE Trans.* 1978, 87.